Optically Illuminated 4H-SiC Terahertz IMPATT Device

M. Mukherjee and N. Mazumder

Department of Applied Physics, International Institute of Information Technology, Visva Bharati University, X-1, 8/3, Block EP, Sector V Salt Lake Electronics Complex, Kolkata 700091, INDIA

The dynamic properties of a 4H-SiC DDR (p^+ p n n^+ type) IMPATT diode operating at 0.5 THz region are studied through DC and small-signal analysis. The study indicates that 4H-SiC IMPATT is capable of generating high RF power (P_{RF}) (2.70 W) at 0.515 terahertz with high efficiency (12 %). However, the parasitic series resistance is found to produce a 7 % reduction in the negative conductance and the P_{RF} of the diode. The effect of photo-illumination on the device is also investigated by studying the role of enhanced saturation current on the THz frequency performance of this IMPATT device. A modified double iterative simulation technique developed by the authors is used for this purpose. It is found that (i) the negative conductance and (ii) the negative resistance of the device decrease, while, the frequency of operation and the device quality factor shift upward with increasing saturation current. The upward shift in operating frequency is found to be more (~ 65 GHz) when the device performance is controlled by the hole saturation current rather than by the electron dominated saturation current. These results thus indicate that 4H-SiC DDR IMPATT diode is highly photo-sensitive even at THz range of frequencies.

1. Introduction

The terahertz (THz) regime (0.1-10 THz) is rich with emerging possibilities in remote sensing, imaging and communications, with unique applications for detecting hidden biological weapons and explosives. Since the last decade, scientists working in this area are showing significant interest to develop solid state sources that may generate THz power. Among all two-terminal semiconductor devices (Gunn, IMPATT, TRAPATT, BARITT etc.), IMPATT[1] devices have already emerged as the most efficient solid state sources that can deliver highest RF power even at 300 GHz [1]. For realizing higher RF power (P_{RF}) from an IMPATT device, one should choose a

semiconductor material that has higher values of critical electric field (E_c) and saturated carrier drift velocity (v_s), since the P_{RF} of an IMPATT device is proportional to $E_c^2 . v_s^2$. Although the conventional IMPATT diodes fabricated on GaAs (Gallium Arsenide) and Si (Silicon) are found to be reliable, these are limited by power and operating frequencies due to the fundamental limitations of the material parameters. On the other hand, wide band gap semiconductor like 4H-SiC (Silicon Carbide) has excellent material properties that can be explored to develop high power IMPATT devices. The authors have, therefore, designed IMPATT diodes based on 4H-SiC, since this material offers (i) 10 times higher E_c, (ii) 2 times higher v_s and (iii) 3 times the thermal conductivity, in comparison to those of Si and GaAs as given in (Table 1) .

Table (1): Material parameters of 4H-SiC, GaAs and Si

	4H-SiC	GaAs	Si
Band Gap Energy (E_g) (eV)	3.26	1.43	1.12
Thermal Conductivity (W/cm-K)	4	0.50	1.50
Electron saturation velocity (v_s) (cm/sec)	2.2×10^7 *	1×10^7	1×10^7
Breakdown field (E_C) (V/cm)	3.5×10^6	4×10^5	3×10^5

* measured perpendicular to c-axis

4H-SiC has an energy band gap approaching 3.3 eV at room temperature, enabling the devices based on this material to support peak internal electric fields (E_c) about ten times higher than Si and GaAs. Higher E_c results in higher breakdown voltage, an essential criterion of a device for generating high power. Higher E_c also permits incorporation of higher doping level (N_D) in the depletion layer of the device, which in turn, reduces the width of the active region. That means, device layers can be made very thin. The transit time of carriers becomes very small in a thin layered semiconductor if the carrier drift velocity is high. The material parameters of 4H-SiC are favorable for realizing smaller transit time. This feature in a 4H-SiC IMPATT diode makes it a potential candidate for operation in the THz range of frequencies, a region unapproachable by conventional IMPATTs due to the high frequency limitations imposed by the material parameters. Further, the high value of thermal conductivity for SiC provides better thermal stability for high power operation of such devices.

Only a few experimental and theoretical studies on 4H-SiC IMPATT diodes have been reported so far [2-4]. Simulation results, reported by Yuan et

al, predicted a maximum power output of 150 W at 35 GHz with 23% efficiency at a dc bias current density of 9.5 kA/ cm^2 [2]. Vassilevski *et.al* fabricated a 4H-SiC IMPATT diode with p^+ n n^+ doping profile and obtained a pulsed power of about 300 mW at X-band frequencies [4].

However, there is still an emergent need for developing solid state high power IMPATT oscillators for operation in the THz region. To meet this gradual demand, the authors have simulated and studied the dc and small signal behavior of a DDR^2 (p^+ p n n^+ type) 4H-SiC IMPATT diode suitable for operation at THz frequency range. The schematic diode structure and doping profile of the designed DDR diode is shown in Fig. (1).

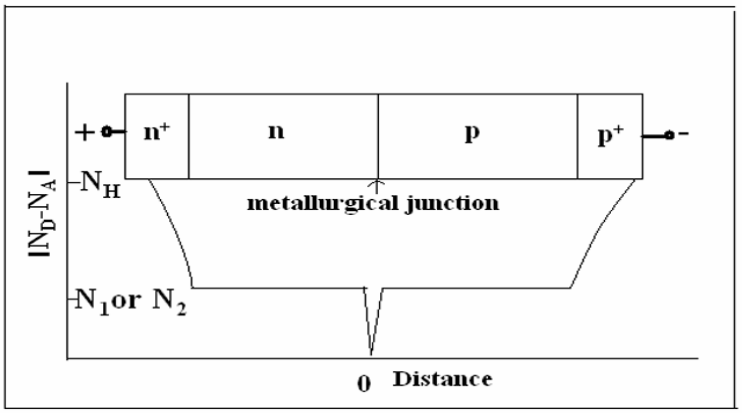

Fig.(1): Schematic diode structure and doping profile of a flat profile DDR IMPATT diode (N_1 or N_2 is flat epilayer doping concentration and N_H is substrate doping concentration).

Optical control of the dynamic properties of IMPATT devices at THz frequency range can have tremendous application in advanced radars and space-communication systems. IMPATT oscillators used as THz sources in spacecrafts may be subjected to interstellar radiation that can produce appreciable changes in the performance of the oscillators. Basic process involved is that, when a photon (due to optical /other radiation) of energy hν greater than the band gap of the semiconductor is absorbed at the edges of the reversed biased p-n junction of an IMPATT diode, creation of additional electron-hole pairs takes place within the active region of the diode. These photo-generated carriers give rise to photocurrent and thereby enhance the existing thermal leakage current in the IMPATT diode. The enhanced leakage current alters the avalanche phase delay in the diode, which subsequently modifies the phase and magnitude of terminal current in the device oscillator circuit. The previous experimental [5-6] as well as theoretical [7-9] studies on

optically illuminated IMPATT diodes indicate that photo-generated carriers reduce the efficiency and power output of the devices, but increase the tuning range of the devices in the mm-wave frequency band.

This paper will present the results of simulated design of 4H-SiC based DDR IMPATT diode having flat doping profile, optimized for THz frequency operation. The authors have also assessed the performance of the THz IMPATT oscillator under optical illumination and the results are reported in the present article.

2. Computer Simulation Method:

The IMPATT diode is basically a p-n junction diode that operates when it is reverse-biased to avalanche breakdown condition. The active layer of a reverse biased p-n junction is shown in Fig. (2). A one-dimensional model of the p-n junction has been considered in the present analysis. The following assumptions have been made in the simulation of dc and small signal behavior of 4H-SiC DDR IMPATT diode: (i) the electron and hole velocities have been taken to be saturated and independent of the electric field throughout the space-charge layer, (ii) the effect of carrier space-charge has been considered, and (iii) the effect of carrier diffusion has been neglected.

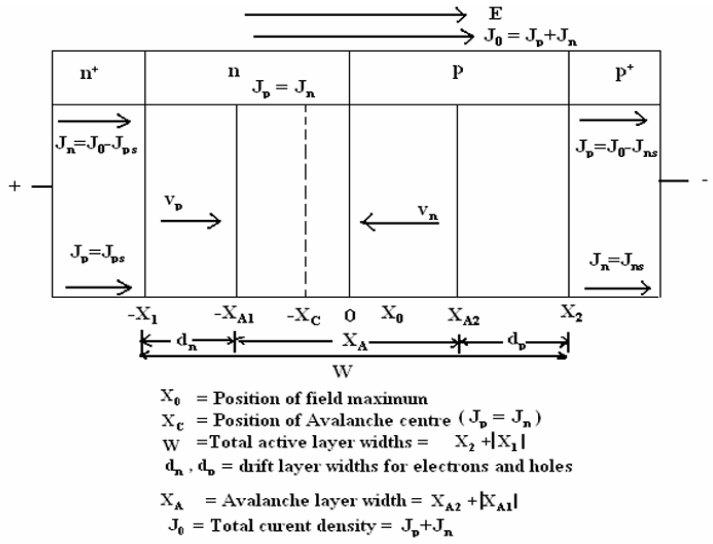

Fig.(2): The active layer of a reverse biased p-n junction.

2.1. DC Analysis:

The dc method, described in details elsewhere [10], considers a generalized (n^{++} n p p^{++}) structure. Here, n^{++} and p^{++} are highly doped substrates and n and p are epilayers. Summarily, in the dc method, the computation starts from the field maximum near the metallurgical junction.

The distribution of dc electric field and carrier currents in the depletion layer are obtained by a double-iterative simulation method, which involves iteration over the magnitude of field maximum (E_m), and its location in the depletion layer. The method is used for a simultaneous solution of Poisson and carrier continuity equations at each point in the depletion layer. The field boundary conditions are given by,

$$E(-x1) = 0 \text{ and } \quad E(+x2) = 0 \qquad (1)$$

Here $-x_1$ and x_2 represent the edges of the depletion layer in n and p regions, respectively.

The boundary conditions for normalized current density P(x), are given by,

$$P(-x_1) = (2/M_p - 1) \quad \text{and} \quad P(x_2) = (1 - 2/M_n) \qquad (2)$$

Where: $M_n = J/J_{ns}$, $M_p = J/J_{ps}$ where J_{ns} and J_{ps} are electron and hole leakage current densities, respectively.

M_p and M_n are hole and electron current multiplication factors, respectively.

$P = (J_p - J_n)/J$, where J_p =hole current density, J_n = electron current density and J = total current density.

Thus, the dc field and carrier current profiles are obtained by solving Poisson and carrier continuity equations, when boundary conditions (1) and (2) are satisfied. The realistic field dependence of electron and hole ionization rates, carrier mobility, and the saturated drift velocities of electron ($v_{s,n}$) and hole ($v_{s,p}$) are used in the computation for the profiles of electric field and carrier currents.

The d.c. to mm-wave conversion efficiency (η) [11] is calculated from the approximate formula,

$$\eta\ (\%) = (VD \times 100)\ /(\pi \times VB) \qquad (3)$$

where, V_D = voltage drop across the drift region. Also, $V_D = V_B - V_A$, where, V_A = voltage drop across the avalanche region, and, V_B = breakdown voltage.

Avalanche breakdown occurs in the junction when the electric field is large enough such that the charge multiplication factors (M_n, M_p) become infinite. The breakdown voltage is calculated by integrating the spatial field profile over the total depletion layer width, i.e.,

$$x_2$$

$$V_B = \int_{-x_1} E(x)\, dx \qquad (4)$$

where, $-x_1$ = n-side depletion layer width
and, $+x_2$ = p-side depletion layer width
The results of the dc analysis are then used in the small signal analysis, described briefly in the next sub-section.

2.2. Small Signal Analysis:

The small signal analysis of the IMPATT diode provides insight into the high frequency performance of the diode. The range of frequencies exhibiting negative conductance of the diode can easily be computed by Gummel-Blue method [12]. From the dc field and current profiles, the spatially dependent ionization rates that appear in the Gummel-Blue equations are evaluated, and fed as input data for the small signal analysis. The edges of the depletion layer of the diode, which are fixed by the dc analysis, are taken as the starting and end points for the small signal analysis. On splitting the diode impedance Z (x,ω) obtained from Gummel–Blue method, into its real part R (x,ω) and imaginary part X (x,ω), two differential equations are framed [10]. A double-iterative simulation scheme incorporating modified Runge-Kutta method is used to solve these two equations simultaneously. The small signal integrated parameters like negative conductance (-G), susceptance (B), impedance (Z), frequency band width, and the quality factor (Q) of the diode are obtained satisfying the boundary conditions derived elsewhere [7].

2.2.1 Small Signal Device Parameters

The simulation method provides the high-frequency negative resistance and negative reactance profiles in the space-charge layer of the device. The diode negative resistance ($-Z_R$) and reactance ($-Z_x$) are computed through numerical integration of the -R (x) and -X (x) profiles over the active space-charge layer.

Thus,

$$-Z_R = \int_{-x_1}^{x_2} -R\, dx, \qquad \text{and} \qquad -Z_X = \int_{-x_1}^{x_2} -X\, dx$$

The diode impedance Z is given by,

$$Z(\omega) = \int_{-x_1}^{x_2} Z(x,\omega)\, dx = -Z_R + jZ_X \qquad (5)$$

The diode admittance is expressed as,

$$Y = 1/ Z = -G + jB = 1/ (-Z_R + j Z_X)$$

or,

$$-G = -Z_R /((Z_R)^2 + (Z_X)^2) \text{ and } B = Z_X / ((Z_R)^2 + (Z_X)^2) \quad (6)$$

It may be noted that both –G and B are normalized to the area of the diode.

The avalanche frequency (f_a) is the frequency at which the imaginary part, susceptance (B) of the admittance changes its nature from inductive to capacitive. Again, it is the minimum frequency at which the real part, conductance (G) of the admittance becomes negative. At the avalanche frequency oscillation starts to build up in the circuit.

The small signal quality factor (Q) is defined as the ratio of the imaginary part of the admittance to the real part of the admittance (at the peak frequency), i.e.,

$$-Q_p = (B_p /-G_p)$$

At a given bias current density, the peak frequency (f_p) is the frequency at which the negative conductance of the diode is a maximum, and the quality factor is a minimum.

At resonance, the maximum RF power output (P_{RF}) from the device is obtained from the expression [13]:

$$P_{RF} = (V_{RF}{}^2 .G_P. A)/2, \quad (7)$$

where V_{RF} (amplitude of the RF swing) is taken as $V_B/5$, assuming a small signal (20%) modulation of the breakdown voltage V_B and A is the area of the diode. The diode negative conductance at the optimum frequency ($-G_p$) is normalized to the area of the diode. The role of parasitic positive series resistance is also considered for calculating realistic values of P_{RF}.

2.3. Simulation Technique for Studying the Illumination Effect

The leakage current (J_s), entering the depletion region of the reversed biased p-n junction of an IMPATT diode, is normally due to thermally generated electrons and holes [$J_s = J_{ns\ (th)} + J_{ps\ (th)}$] and it is so small that current multiplication factor $M_{n,p} = J_o /[J_{ns\ (th)}$ or $J_{ps\ (th)}]$, [J_o = bias current density] can be considered to be infinitely large. Thus, the enhancement of the leakage current under optical illumination of the devices is manifested as the lowering of $M_{n,p}$. The composition of the leakage current (electron versus hole photocurrent) plays a vital role in controlling the microwave properties of the optically illuminated IMPATTs. In a DDR IMPATT structure (p^+ p n n^+ type), the composition of photocurrent may be altered by shining a laser beam selectively on the p^+ or n^+ side of the device through fabricated optical windows

of appropriate diameter, keeping the diode mounted in a microwave cavity. Thus, the electron saturation current and also the hole saturation current might be enhanced separately, which would produce changes in the THz performance of the IMPATT.

Under optical illumination, the expression for electron current multiplication factor changes to
$M_n = J_o / [J_{ns\ (th)} + J_{ns\ (opt)}]$, $[J_{ns\ (opt)}$ = saturation current due to photoelectrons].

Thus, the photoelectrons reduce the value of M_n, while the value of M_p remains unchanged.

Again, under optical illumination the expression for hole current multiplication factor changes to
$M_p = J_o / [J_{ps\ (th)} + J_{ps\ (opt)}]$, $[J_{ps\ (opt)}$ = saturation current due to photo generated holes].

So, the photo generated holes reduce the value of M_p, while the value of M_n remains unchanged.

In order to assess the role of leakage current in controlling the dynamic properties of IMPATT oscillator at THz frequencies, simulation studies are carried out by the authors on the effect of M_n (keeping M_p very high ~ 10^6) and M_p (keeping M_n very high ~ 10^6) on (i) the small signal admittance characteristics, (ii) the negative resistivity profiles, and (iii) the device quality factor (Q) of flat profile 4H-SiC DDR IMPATT. The details of mathematical calculations based on modified boundary conditions due to enhancement of leakage current are described elsewhere [7].

3. Design Parameters:

4H-SiC DDR IMPATT diode with flat doping profile has been designed and studied following the dc and small signal methods described above. The experimental values of material parameters, viz., realistic field dependence of carrier ionization rates [14], saturated drift velocities of charge carriers [15-16], and carrier mobility [17] in 4H-SiC have been incorporated in the analysis. The junction temperature has been assumed to be 300K. The diode has been considered to be a circular chip of 8 μm diameter. The device dimensions, doping and current densities of the designed diode are listed in Table 2. The device structural parameters and the current density have been optimized for THz operation through several computer runs.

Table (2): Design parameters of 4H-SiC DDR IMPATT Diode at THz frequency region

Diode type	Flat epilayer Doping conc. (n and p regions) (10^{23} m^{-3})	Width of the flat epilayer (n and p regions) (μm)	Current density (10^9 A m^{-2})
flat doping profile	9.5	0.16	6.0

4. Results and Discussions

The optimized design parameters of the unilluminated 4H-SiC DDR IMPATT diode for which M_n and M_p are both large (=10^6) are summarized in Table 2. The dc and high frequency properties of this designed THz diode are reported in Table (3). It is observed from Table 3 that the designed diode is capable of generating 2.7 W RF power with an efficiency of 12% at 0.515 THz frequency.

Table (3): MM-wave properties of 4H-SiC DDR IMPATT Diode at THz region.

Diode parameters	4H-SiC DDR IMPATT
E_m (10^8 V m^{-1})	4.3
V_B (V)	96.0
V_D/V_B (%)	37.7
η(%)	12.0
f_a (THz)	0.425
f_p (THz)	0.515
$-G_p$ (10^6 S m^{-2})	290.0
$-Q_p$	1.95
P_{RF} (W)	2.7

The value of parasitic series resistance (R_S) for SiC THz IMPATT is calculated following a method described elsewhere [18] and its effect on $-G_P$ and P_{RF} are shown in Fig. (3 and 4), respectively. It is interesting to note that due to the presence of R_S (~ 4.2 Ω), the values of $-G_P$ as well as P_{RF} of the unilluminated diodes reduces approximately by 7.0%.

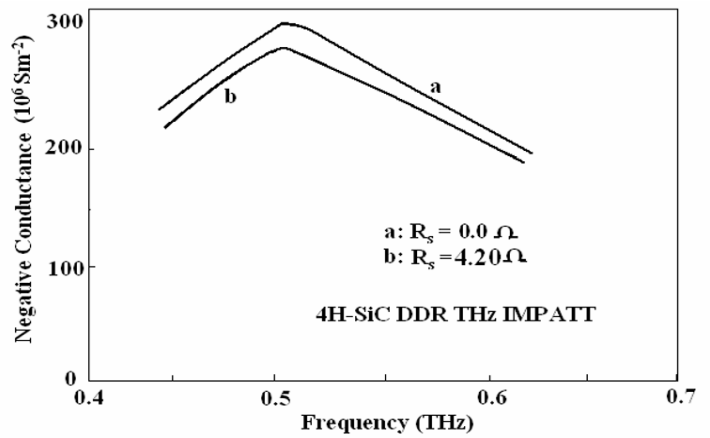

Fig.(3): Plots of negative conductance versus frequency (with and without R_S) for the unilluminated 4H-SiC DDR IMPATT diode operating at THz frequency region.

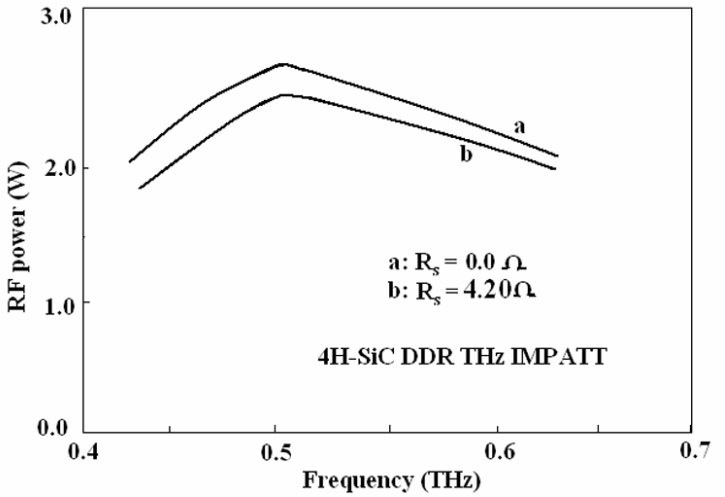

Fig.(4): Plots of RF-power versus frequency (with and without R_S) for the unilluminated 4H-SiC DDR IMPATT diode operating at THz frequency region.

Table (4) shows the effect of electron and hole dominated photocurrent on the high frequency properties of 4H-SiC DDR THz IMPATT. In Figs. (5 and 6), plots of -G versus B for 4H-SiC DDR IMPATT for different values of M_n and M_p are shown. The graphs show that the values of $|-G_P|$ of the diode decreases with the lowering of M_n and M_p. At the same time, the frequency range over which the device exhibits negative conductance, shifts towards higher frequencies with the lowering of M_n and M_p. The output data for illuminated flat profile DDR IMPATT diode (Table (4)) indicate that the value

of negative conductance at peak frequency $|-G_P|$ decreases by 6 % when M_n reduces from 10^6 to 10, while $|-G_P|$ decreases by 45 % for the same decrease of M_p from 10^6 to 10 at a particular current density ($J_0 = 6 \times 10^9$ A m^{-2}).

Table (4): Variation of small signal parameters of 4H-SiC THz DDR IMPATT Diode under optical illumination.

M_n	M_p	f_p (THz)	$-G_p$ (10^6 Sm^{-2})	$-Z_{Rp}$ (10^{-10} Ω m^2)	RF Power (W)	$-Q_P$
$1x10^6$	$1x\ 10^6$	0.515	290.0	5.45	2.70	1.95
100	,,	0.517	287.7	5.40	2.65	2.10
50	,,	0.522	282.8	5.33	2.60	2.13
10	,,	0.540	272.7	4.63	2.51	2.3
$1x10^6$	100	0.520	271.0	5.20	2.49	2.21
,,	50	0.530	258.6	4.63	2.38	2.40
,,	10	0.580	160.0	2.10	1.47	4.1

It is further evident from Figs. (5 and 6) that for THz operation of the 4H-SiC IMPATT, a lowering of M_p causes more upward shift in frequency than a corresponding lowering of M_n can make. The same trend is also reflected when we analyse the values of optimum frequencies for different values of M_n and M_p presented in Table 4. It may be seen from the table that the optimum frequency of oscillation (f_P) increases by 5 % (0.515 THz to 0.540 THz) and 12.6% (0.515 THz to 0.580 THz) as M_n and M_p reduce from 10^6 to 10, respectively.

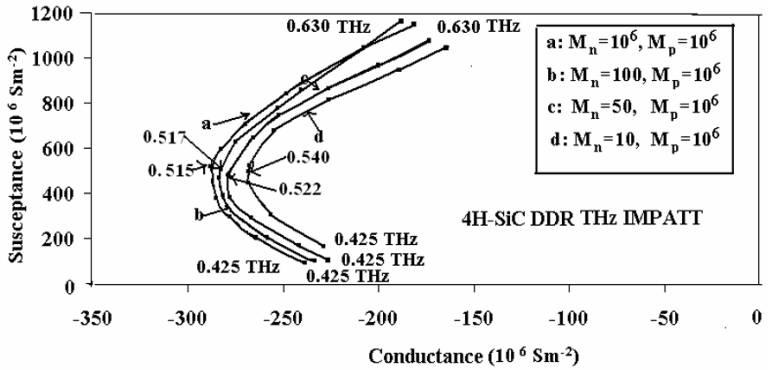

Fig.(5): Conductance versus Susceptance plots of the unilluminated 4H-SiC flat profile DDR IMPATT diode (a) and the illuminated diode (b-d) for different values of M_n.

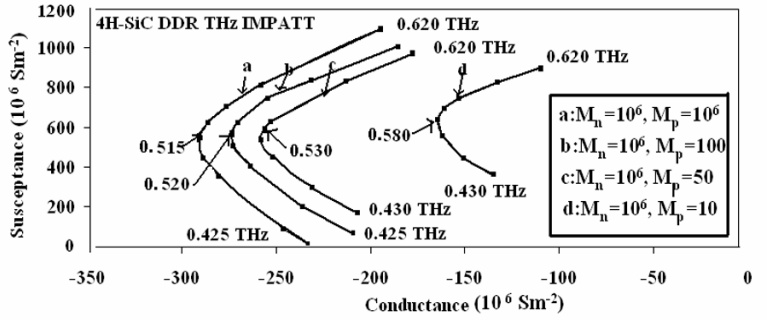

Fig.(6): Conductance versus Susceptance plots of the unilluminated 4H-SiC flat profile DDR IMPATT diode (a) and the illuminated diode (b-d) for different values of M_p.

Figure (7 and 8) show the negative resistivity profiles at the peak frequencies corresponding to different values of M_n (M_p =10^6) and M_p (M_n = 10^6), respectively for 4H-SiC DDR IMPATT. In each case, the profiles are characterized by two negative resistivity peaks in the middle of the two drift layers of the diode interspaced by a dip in the avalanche region. It is observed from the figures that due to the enhancement of electron and hole photocurrents, the negative resistivity peaks in the electron and hole drift layers are depressed gradually. It is also found that the decrease in the magnitude of the negative resistivity peaks are more pronounced for variation of M_p corresponding to hole dominated photocurrent than for the same variation of M_n corresponding to electron dominated photocurrent.

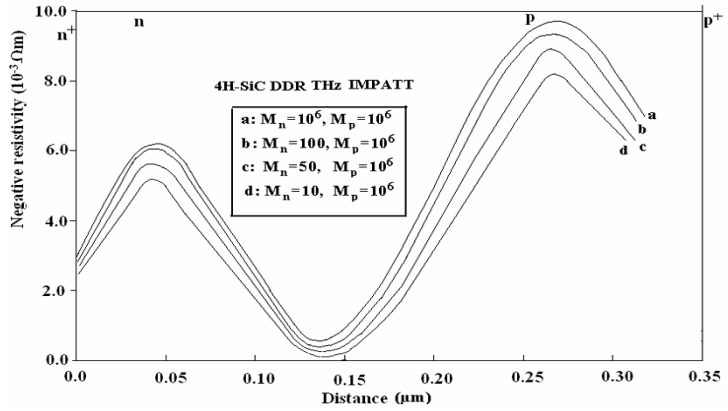

Fig.(7): Variation of negative resistivity profiles of the unilluminated 4H-SiC flat profile DDR IMPATT diode (a) and the illuminated diode (b-d) for different values of M_n, and corresponding values of optimum frequencies, f_P:

a: $M_n = 10^6$, $M_P = 10^6$, $f_P = 0.515$ THz;

b: $M_n = 100$, $M_P = 10^6$, $f_P = 0.517$ THz; c: $M_n = 50$, $M_P = 10^6$, $f_P = 0.522$ THz; d: $M_n = 10$, $M_P = 10^6$, $f_P = 0.540$ THz.

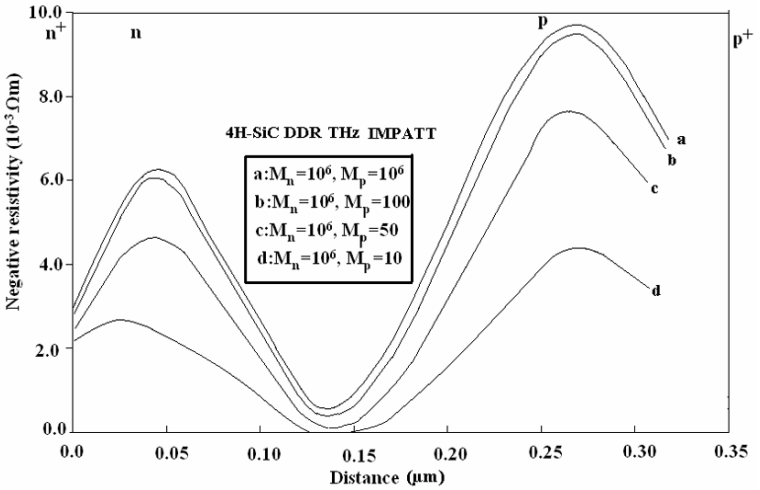

Fig.(8): Variation of negative resistivity profiles of the unilluminated 4H-SiC flat profile DDR IMPATT diode (a) and the illuminated diode (b-d) for different values of M_p, and corresponding values of optimum frequencies, f_P:
a: $M_p = 10^6$, $M_n = 10^6$, $f_P = 0.515$ THz;
b: $M_p = 100$, $M_n = 10^6$, $f_P = 0.520$ THz; c: $M_p = 50$, $M_n = 10^6$, $f_P = 0.530$ THz;
d: $M_p = 10$, $M_n = 10^6$, $f_P = 0.580$ THz.

Simulation study also depicts that in case of 4H-SiC DDR IMPATT, as M_n is decreased from 10^6 to 10, there occurs a 15 % decrease in the diode negative resistance ($-Z_{Rp}$). On the other hand, as M_p changes from 10^6 to 10, $-Z_{Rp}$ reduces by 61 % (Table (4)).

The variations of power output with optimum frequency for different values of M_n and M_p are also shown in Table 4. Again, it is found from the study that the magnitude of device quality factor at optimum frequency of oscillation $|-Q_P|$ increases appreciably for a decrease of M_p compared to the same change of M_n values (Table (4)).

The enhancement of leakage currents by electron and hole dominated photocurrents thus lead to a decrease of $-Z_{RP}$, $-G_P$ and P_{RF} along with a simultaneous upward shift of f_P. While the photo generated leakage current dominated by holes modulates the dc and high-frequency properties of the device appreciably, that dominated by electrons has relatively less effect in modulating the same. For the mm-wave Si DDR, it was reported that the

electron saturation current was more dominant in changing the P_{RF} and the f_P [19]. In Si, the electron ionization rate is greater than the hole ionization rate. This means that by controlling the DDR IMPATT action through more ionizing carriers in Si, a higher frequency shift may be achieved. By the same logic it can also be concluded that in 4H-SiC, holes are more ionizing carriers than electrons, since 4H-SiC DDR IMPATT under optical illumination at THz region is more sensitive to hole dominated photocurrent. This relative predominance of hole leakage current in optical control of 4H-SiC DDR IMPATT performance can be attributed to the inequality of the ionization coefficient values in 4H-SiC [3].

5. Conclusions:

A detailed simulation study of the high frequency behavior of 4H-SiC based flat profile DDR IMPATT diode operating at 0.515 THz frequency was reported for the first time. It was found that high RF power (Watt level) might be obtained from 4H-SiC IMPATT with appreciable efficiency even at THz frequency regime. Further, a systematic study was carried out on the effect of optical illumination on 4H-SiC IMPATT device at THz range of frequencies. It was observed that the frequency of oscillation of the device increased gradually under optical illumination. The upward shift of optimum frequency of operation was found to be more (65 GHz) when the performance of the THz 4H-SiC IMPATT was controlled by hole dominated photocurrent, rather than by electron dominated photo current. However, the peak negative conductance and the P_{RF} of the illuminated diodes were found to decrease. It was thus evident from the studies that 4H-SiC DDR IMPATT diode exhibited satisfactory dynamic performance even at THz frequency range, as well as the diode exhibited better response to external radiation. Our findings on the optical control of THz IMPATT may be utilized for realizing optically integrated THz modules for applications in interstellar explorers.

Acknowledgment:

The authors wish to express their gratitude to the Director, International Institute of Information Technology, Kolkata for his interest in the work.

References

1. R. J. Trew, *IEEE Trans. Electron Dev.* **52**, 638 (2005).

2. L Yuan, M. R. Melloch Jr., J A Cooper and K. J. Webb, *IEEE /Cornell Conf. Advanced Concepts in High Speed Semiconductor Devices and Circuit,* Ithaca, NY, August 7-9, (2000)

3. J. H. Zhao, V. Gruzinskis, Y. Luo,M. Weiner, M. Pan, P. Shiktorov, E. Starikov, *Semicond. Sci. Technol*., **15** (11), 1093 (2000).

4. K.V. Vassilevski, A.V. Zorenko, K. Zekentes, K.Tsagaraki, E.Bano, C.Banc and A. A. Lebedev, *Materials Science Forum.* **389-393**, 1353 (2002)

5. H.P. Vyas, R.J. Guttmann and J.M .Borrego, *IEEE Trans Electron Devices* **ED-26**, 232 (1979)

6. A. J. Seeds, J. F. Singleton, S. P. Brunt and J. R. Forrest, *J Lightwave Technol.* **LT-5**, 403 (1987)

7. N. Mazumder, J. P. Banerjee and S. K. Roy, *phys. Stat. solidi. (a)* **116,** 415 (1989)

8. N. Mazumder and S. K. Roy, *Int J Electronics* **71**, 227 (1991)

9. N. Mazumder and S. K. Roy, *phys. Stat. solidi. (a)* **137**, 267 (1993).

10. S. K Roy, J .P. Banerjee and S. P. Pati, *Proc. 4th Conf. on Num. Anal. of Semiconductor Devices. (NASECODE IV) (Dublin: Boole) (Ed. J.H. Miller)* 494 (1985)

11. D. L. Scharfetter and H. K. Gummel, *IEEE Trans. Electron Devices*, **16,** 64 (1969)

12. H. K. Gummel and J. L. Blue, *IEEE Trans. Electron Devices,* **ED –14,** 569 (1967)

13. H. Eisele and G .I. Haddad, *"Microwave Semiconductor Device Physics"*, Ed. S. M. Sze, Wiley, New York, 1997, p. 343

14. A. Konstantinov, Q. Wahab, N. Nordell, U. Linderfelt, *Material. Science Forum*, **264-268**, 513 (1998)

15. A. Khan and J. A. Cooper, *IEEE Trans. Electron Devices* **47**, 269 (2000)

16. www.cree.com

17. *Electronic Archive: New Semiconductor Materials, Characteristics and Properties (online)* www.ioffe.ru/SVA/NSM/Semicond/SiC

18. L. Yuan, *Ph.D. Thesis*, Purdue University, Faculty of Electrical Engineering, Purdue, USA, 2000

19. N. Mazumder and S. K. Roy, *Proceedings of the International Conference on Millimeter waves and Microwaves (ICOMM-90)*, DEAL, Dehradun, India, 19-27 December 1990 (New Delhi, India: Tata McGraw-Hill) 135